Eur. Phys. J. A **29**, 39–42 (2006)
DOI 10.1140/epja/i2005-10295-7

THE EUROPEAN PHYSICAL JOURNAL A

Triple-gluon and triple-quark elastic scatterings and early thermalization

X.-M. Xu[a]

Department of Physics, Shanghai University, Baoshan, 200444 Shanghai, PRC

Received: 23 October 2005 /
Published online: 29 August 2006 –

Abstract. Three-gluon to three-gluon scatterings lead to rapid thermalization of gluon matter created in central Au-Au collisions at RHIC energies. Thermalization of quark matter is studied from three-quark to three-quark scatterings.

PACS. 24.85.+p Quarks, gluons, and QCD in nuclei and nuclear processes – 12.38.Mh Quark-gluon plasma – 12.38.Bx Perturbative calculations – 25.75.Nq Quark deconfinement, quark-gluon plasma production, and phase transitions

1 Introduction

While the energy of nucleus-nucleus collisions increases, the density of initially created partons gets larger and larger. Number density of gluon matter has been required to be more than $30\,\mathrm{fm}^{-3}$ in RHIC Au-Au collisions and may reach $140\,\mathrm{fm}^{-3}$ in LHC Pb-Pb collisions. At such high gluon number densities, new physics processes begin to play an important role and are responsible for some phenomena. Three-gluon to three-gluon scatterings have been shown to lead to rapid thermalization of gluon matter created in RHIC central Au-Au collisions [1]. Thermalization has been studied from parton cascade models [2–4] and in other model attempts [5–12].

To study triple-gluon elastic scatterings, we need to know how frequently the triple-gluon scatterings occur. This is shown by the ratio of three-gluon to two-gluon scattering numbers in the next section. The triple-gluon and triple-quark elastic scatterings and transport equations are given briefly in sects. 3-5, respectively. The summary is in the last section.

2 Ratio of scattering numbers

We estimate the ratio of numbers of scatterings occurring between two gluons or among three gluons at the moment when gluon matter is formed. The counting of scatterings is made for gluons in an anisotropic momentum distribution obtained from HIJING simulation [13] for initial central Au-Au collisions at $\sqrt{s_{NN}} = 200\,\mathrm{GeV}$,

$$f(\mathbf{p}, t_{\mathrm{ini}}) = \frac{1.07 \times 10^6 (2\pi)^{1.5}}{\pi R_A^2 Y(|\mathbf{p}|/\cosh(y) + 0.3)} \times \mathrm{e}^{-|\mathbf{p}|/(0.9\cosh(y)) - (|\mathbf{p}|\tanh(y))^2/8} \bar{\theta}(Y^2 - y^2), \quad (1)$$

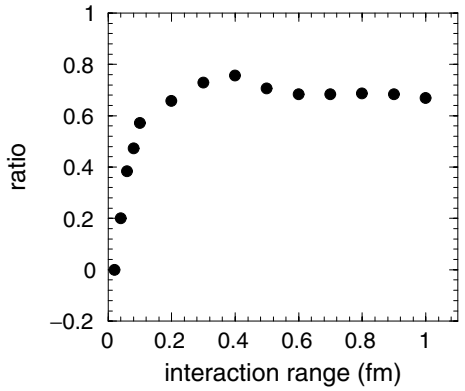

Fig. 1. Ratio of three-gluon scattering to two-gluon scattering numbers *versus* the interaction range.

where $R_A = 6.4\,\mathrm{fm}$, $t_{\mathrm{ini}} = 0.2\,\mathrm{fm}/c$ and the rapidity region $|y| \leq Y = 5$. $\bar{\theta}(x)$ equals 0 for $x < 0$ or 1 for $x \geq 0$. One thousand gluons are generated from the distribution within the cylinder which has a radius of R_A and a longitudinal regime of $-0.2\,\mathrm{fm} < z < 0.2\,\mathrm{fm}$. Then the maxima of the numbers of the two-gluon and three-gluon scatterings are 500 and 333, respectively. We determine a scattering of two gluons when the distance of the two gluons is less than a given interaction range. If three gluons are within a sphere whose center is the center of mass of the three gluons and whose radius equals the given interaction range, a scattering of the three gluons occurs. The ratio of the numbers of the three-gluon scatterings to the two-gluon scatterings at the time t_{ini} is plotted in fig. 1. If the interaction range approaches zero from 0.1 fm, the number of the three-gluon scatterings reduces faster than the two-gluon scatterings; when the interaction range is larger than 0.6 fm, both of the scattering numbers are close to

[a] e-mail: xmxu@xmxucao.sina.net

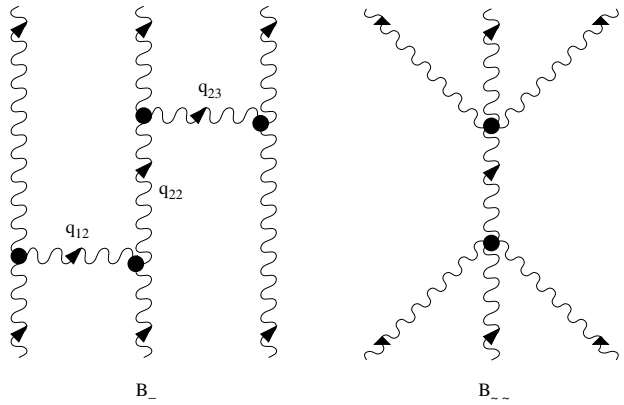

Fig. 2. Scatterings of three gluons.

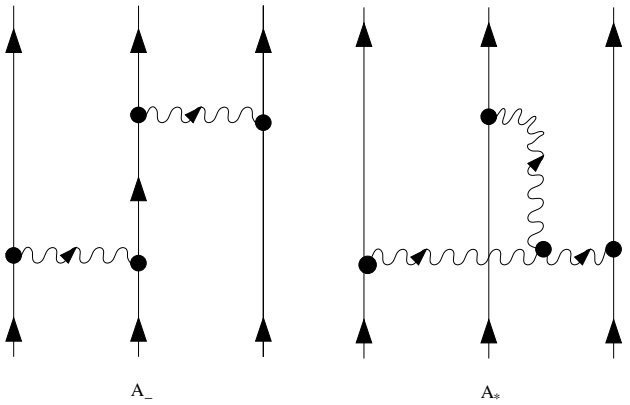

Fig. 3. Scatterings of three quarks.

their maxima; when it is larger than 0.1 fm, the ratio varies around 0.7. The importance of the three-gluon scatterings is verified.

3 Three-gluon to three-gluon scatterings

The triple-gluon elastic scatterings involve many diagrams at order α_s^4 [1] and only two of them are selected to be shown in fig. 2 for illustration. The scattering processes at tree level contain three-gluon and four-gluon couplings. Three incoming gluons interact at different space-time points or at the same space-time point. The squared four-momenta of propagators, q_{12}^2, q_{22}^2 and q_{23}^2, may tend to zero, which causes Coulomb exchange divergence. The divergence is removed with the use of a screening mass. The triple-gluon scattering B_- cannot be thus identified as an iterative process of two successive scatterings of on-shell gluons. Such screening mass is evaluated in the use of a formula in ref. [14].

Squared amplitudes of three-gluon scattering diagrams are derived with Fortran code in the Feynman gauge. Interference terms of different diagrams are also calculated. If a gluon's four-momentum is labeled as $p_i = (E_i, \mathbf{p}_i)$ in the process $g(p_1) + g(p_2) + g(p_3) \to g(p_4) + g(p_5) + g(p_6)$, squared amplitudes are outputted in terms of the following Lorentz-invariant variables, $s_{12} = (p_1 + p_2)^2$, $s_{23} = (p_2 + p_3)^2$, $s_{31} = (p_3 + p_1)^2$, $u_{15} = (p_1 - p_5)^2$, $u_{16} = (p_1 - p_6)^2$, $u_{24} = (p_2 - p_4)^2$, $u_{26} = (p_2 - p_6)^2$, $u_{34} = (p_3 - p_4)^2$ and $u_{35} = (p_3 - p_5)^2$. In derivations, all possible exchanges of final (initial) gluons are also taken into account to obtain different diagrams.

4 Three-quark to three-quark scatterings

We use quark-quark elastic scatterings [15,16] and three-quark to three-quark elastic scatterings [17] to study quark matter which is an ingredient of quark-gluon matter created in central Au-Au collisions at $\sqrt{s_{NN}} = 200\,\mathrm{GeV}$. Quark matter is considered as consisting of only up-quarks and down-quarks and the two kinds of quarks have the same distribution functions. The triple-quark elastic scattering processes are plotted in fig. 3. Exchanges of final (initial) quarks generate forty-two different diagrams. Squared amplitudes for all the diagrams are derived from Fortran code and expressed in terms of s_{12}, s_{23}, s_{31}, u_{15}, u_{16}, u_{24}, u_{26}, u_{34} and u_{35}. The 42 diagrams contribute to the scatterings of three quarks with the same flavor. If one quark's flavor differs from the other two, only 14 diagrams give contributions.

5 Transport equations

A transport equation of Boltzmann type including three-parton to three-parton scatterings is

$$\begin{aligned}
&\frac{\partial f_1}{\partial t} + \mathbf{v}_1 \cdot \nabla_{\mathbf{r}} f_1 = -\frac{g}{2E_1 g_{22}} \\
&\times \int \frac{\mathrm{d}^3 p_2}{(2\pi)^3 2E_2} \frac{\mathrm{d}^3 p_3}{(2\pi)^3 2E_3} \frac{\mathrm{d}^3 p_4}{(2\pi)^3 2E_4} (2\pi)^4 \delta^4(p_1 + p_2 - p_3 - p_4) \\
&\times |\mathcal{M}_{2\to 2}|^2 [f_1 f_2 (1 \pm f_3)(1 \pm f_4) - f_3 f_4 (1 \pm f_1)(1 \pm f_2)] - \frac{g^2}{2E_1 g_{33}} \\
&\times \int \frac{\mathrm{d}^3 p_2}{(2\pi)^3 2E_2} \frac{\mathrm{d}^3 p_3}{(2\pi)^3 2E_3} \frac{\mathrm{d}^3 p_4}{(2\pi)^3 2E_4} \frac{\mathrm{d}^3 p_5}{(2\pi)^3 2E_5} \frac{\mathrm{d}^3 p_6}{(2\pi)^3 2E_6} \\
&\times (2\pi)^4 \delta^4(p_1 + p_2 + p_3 - p_4 - p_5 - p_6) |\mathcal{M}_{3\to 3}|^2 \\
&\times [f_1 f_2 f_3 (1 \pm f_4)(1 \pm f_5)(1 \pm f_6) \\
&- f_4 f_5 f_6 (1 \pm f_1)(1 \pm f_2)(1 \pm f_3)], \qquad (2)
\end{aligned}$$

where g is the color spin degeneracy factor, the velocity for massless partons $v_1 = 1$, $g_{22} = n'_{\mathrm{out}}!$ and $g_{33} = n_{\mathrm{in}}! n_{\mathrm{out}}!$ where n'_{out} (n_{out}) is the number of identical final partons of $2 \to 2$ ($3 \to 3$) scatterings and n_{in} for the $3 \to 3$ scatterings is the number of identical initial partons except the parton in the distribution function f_1. $|\mathcal{M}_{2\to 2}|^2$ and $|\mathcal{M}_{3\to 3}|^2$ represent squared amplitudes of $2 \to 2$ and $3 \to 3$ parton scatterings, respectively. The $3 \to 3$ scattering processes involve a larger phase space than the $2 \to 2$ scattering processes.

Anisotropy of a parton momentum distribution as in eq. (1) can be eliminated by elastic scatterings among partons. The transport equation is solved from the time

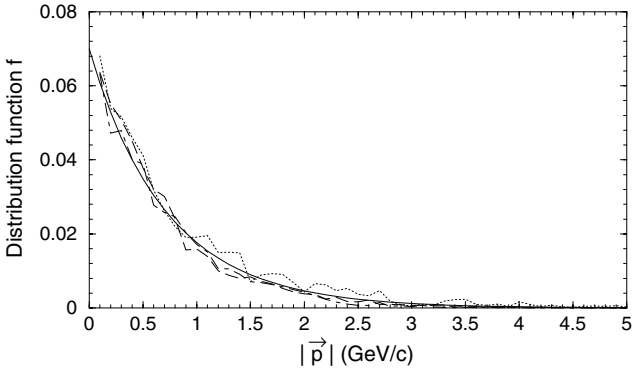

Fig. 4. Gluon distribution functions *versus* momentum at $t_{\rm iso} = 0.65\,{\rm fm}/c$. The dotted, dashed and dot-dashed curves correspond to the angles $\theta = 0^{\rm o}, 45^{\rm o}, 90^{\rm o}$, respectively. The solid curve represents the thermal distribution function given by eq. (3).

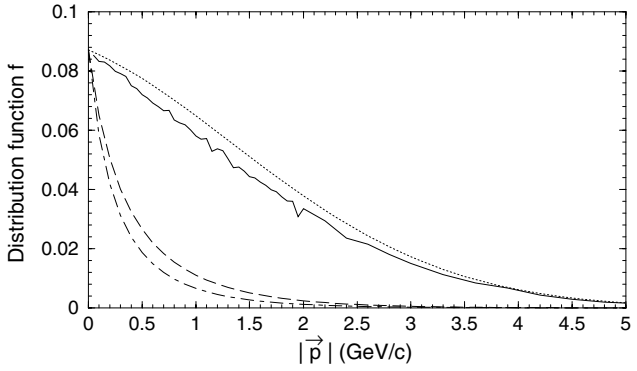

Fig. 5. Gluon distribution functions at $t_{\rm ini} = 0.2\,{\rm fm}/c$ are shown by the dotted, dashed and dot-dashed curves which correspond to the angles $\theta = 0^{\rm o}, 45^{\rm o}, 90^{\rm o}$, respectively. The $2 \to 2$ gluon scatterings result in the solid curve for the gluon distribution function at $\theta = 0^{\rm o}$ at $t_{\rm iso} = 0.65\,{\rm fm}/c$.

$t_{\rm ini}$ when anisotropic parton matter is formed and until the time $t_{\rm iso}$ when local momentum isotropy is established. For gluon matter, gluon distribution functions at $t_{\rm iso} = 0.65\,{\rm fm}/c$ in three different directions are shown in fig. 4 by the dotted, dashed and dot-dashed curves. The three directions correspond to the angles $\theta = 0^{\rm o}, 45^{\rm o}, 90^{\rm o}$ with respect to an incoming gold beam direction. The solution of the transport equation at $t_{\rm iso}$ exhibits similar momentum dependences in different directions relative to the beam direction. Such dependences can thus be fitted to the Jüttner distribution which differs substantially from the anisotropic momentum distribution given by eq. (1),

$$f(\mathbf{p}, t_{\rm iso}) = \frac{\lambda}{{\rm e}^{|\mathbf{p}|/T} - \lambda}\,, \tag{3}$$

where temperature $T = 0.75\,{\rm GeV}$, fugacity $\lambda = 0.065$, the thermalization time of $t_{\rm iso} - t_{\rm ini} = 0.45\,{\rm fm}/c$ for gluon matter. When quark matter evolves independently, $2 \to 2$ and $3 \to 3$ quark scatterings result in a thermal state with $T = 0.59\,{\rm GeV}$, $\lambda = 0.04$ and $t_{\rm iso} - t_{\rm ini} = 1.8\,{\rm fm}/c$ for quark matter [17]. The thermalization times for gluon matter and quark matter are very different.

To definitely realize a role of the $3 \to 3$ gluon scatterings, the gluon distribution function at the time $t_{\rm iso} = 0.65\,{\rm fm}/c$ resulted only from the $2 \to 2$ gluon scatterings is shown as a solid curve in fig. 5. The small discrepancy of the solid and the dotted curves exhibits a small variation of the gluon distribution function at the angle $\theta = 0^{\rm o}$. The gluon distribution functions at the two angles $\theta = 45^{\rm o}, 90^{\rm o}$ at $t_{\rm iso} = 0.65\,{\rm fm}/c$ are very close to the dashed and dot-dashed curves and are thus not plotted. The variation of gluon distribution function resulted from the $2 \to 2$ gluon scatterings is small in the forward direction and even negligible away from this direction. Therefore, in the thermalization driven by both the $2 \to 2$ and $3 \to 3$ gluon scatterings, the gluon distribution variation from the anisotropic form to the thermal state is mainly caused by the $3 \to 3$ gluon scatterings.

6 Conclusions

We have studied thermalization of gluon matter and quark matter with the three-parton to three-parton elastic scatterings. The three-gluon elastic scattering processes give a considerably larger variation of the gluon distribution function than the two-gluon elastic scattering processes while the gluon number density is high. The triple-gluon scatterings are important at RHIC energies and yield the effect of rapid thermalization. The triple-quark scatterings give a variation of quark distribution function comparable to the one that resulted from the quark-quark scatterings. Quark matter itself cannot thermalize rapidly at RHIC energies.

This work was supported in part by the National Natural Science Foundation of China under Grant No. 10135030 and No. 10510201129, in part by the Shanghai Education Committee Research Fund No. 04AB04 and in part by the CAS Knowledge Innovation Project No. KJCX2-SW-N02.

References

1. X.-M. Xu, Y. Sun, A.-Q. Chen, L. Zheng, Nucl. Phys. A **744**, 347 (2004).
2. K. Geiger, Phys. Rev. D **46**, 4965; 4986 (1992).
3. G.R. Shin, B. Müller, J. Phys. G **29**, 2485 (2003).
4. Z. Xu, C. Greiner, Phys. Rev. C **71**, 064901 (2005).
5. E. Shuryak, Phys. Rev. Lett. **68**, 3270 (1992).
6. K.J. Eskola, M. Gyulassy, Phys. Rev. C **47**, 2329 (1993).
7. R.S. Bhalerao, G.C. Nayak, Phys. Rev. C **61**, 054907 (2000).
8. G.C. Nayak, A. Dumitru, L. McLerran, W. Greiner, Nucl. Phys. A **687**, 457 (2001).
9. S.M. Wong, Phys. Rev. C **54**, 2588 (1996).
10. R. Baier, A.H. Mueller, D. Schiff, D.T. Son, Phys. Lett. B **502**, 51 (2001).
11. S.G. Matinyan, B. Müller, D.H. Rischke, Phys. Rev. C **57**, 1927 (1998).

12. See in these proceedings the papers by A.H. Mueller, A.I. Shoshi, S.M.H. Wong; G.D. Moore; M. Strickland; F. Gelis, K. Kajantie, T. Lappi.
13. P. Lévai, B. Müller, X.-N. Wang, Phys. Rev. C **51**, 3326 (1995).
14. T.S. Biró, B. Müller, X.-N. Wang, Phys. Lett. B **283**, 171 (1992).
15. R. Cutler, D. Sivers, Phys. Rev. D **17**, 196 (1978).
16. B.L. Combridge, J. Kripfganz, J. Ranft, Phys. Lett. B **70**, 234 (1977).
17. X.-M. Xu, R. Peng, H.J. Weber, Phys. Lett. B **629**, 68 (2005).